

Ablation of metals with picosecond laser pulses: Evidence of long-lived nonequilibrium conditions at the surface

E. G. Gamaly,^{1,2,*} N. R. Madsen,¹ M. Duering,³ A. V. Rode,^{1,2} V. Z. Kolev,^{1,2} and B. Luther-Davies^{1,2}

¹*Laser Physics Centre, Research School of Physical Sciences and Engineering, The Australian National University, Canberra, ACT 0200, Australia*

²*Centre for Ultra-high Bandwidth Devices for Optical Systems, Australian National University, Canberra, ACT 0200, Australia*

³*Fraunhofer Institute for Laser Technique, Steinbachstrasse 15, D-52074 Aachen, Germany*

(Received 18 August 2004; revised manuscript received 23 December 2004; published 6 May 2005)

We report here experimental results on laser ablation of metals in air and in vacuum in similar irradiation conditions. The experiments revealed that the ablation thresholds in air are less than half those measured in vacuum. Our analysis shows that this difference is caused by the existence of a long-lived transient nonequilibrium surface state at the solid-vacuum interface. The energy distribution of atoms at the surface is Maxwellian-like but with its high-energy tail truncated at the binding energy. We find that in vacuum the time needed for energy transfer from the bulk to the surface layer to build the high-energy tail, exceeds other characteristic timescales such as the electron-ion temperature equilibration time and surface cooling time. This prohibits thermal evaporation in vacuum for which the high-energy tail is essential. In air, however, collisions between the gas atoms and the surface markedly reduce the lifetime of this nonequilibrium surface state allowing thermal evaporation to proceed before the surface cools. We find, therefore, that the threshold in vacuum corresponds to nonequilibrium ablation during the pulse, while thermal evaporation after the pulse is responsible for the lower ablation threshold observed in air. This paper provides direct experimental evidence of how the transient surface effects may strongly affect the onset and rate of a solid-gas phase transition.

DOI: 10.1103/PhysRevB.71.174405

PACS number(s): 61.82.Bg, 52.38.Mf, 64.70.Hz

I. INTRODUCTION

Many experimental and theoretical studies of the ablation threshold and the ablation rate for metals irradiated with picosecond laser pulses clearly demonstrate the presence of two different ablation regimes depending on the pulse duration.^{1–10} For pulses longer than about 100 ps, the surface temperature is determined by the thermal diffusivity of the material and hence the ablation proceeds in equilibrium conditions. The threshold fluence F_{thr} , sometimes referred as the damage threshold, increases with pulse duration t_p according to the relation $F_{\text{thr}} \propto t_p^{1/2}$. However for subpicosecond pulses ablation proceeds in nonequilibrium conditions because the pulse duration is shorter than both the electron-to-lattice energy transfer time, which is of the order of 1–10 ps, as well as the electron heat conduction time. Hence the electrons cool without transferring energy to the lattice.^{6–10} In this regime the ablation threshold becomes independent of the pulse duration. However, the transition observed experimentally from the ablation threshold expected for the nonequilibrium regime to the thermal regime occurs at unexpectedly large pulse durations, for example, up to ~ 100 ps in gold.^{2,10} This indicates that for some reason, which is not yet fully understood, the thermal mechanism does not contribute to the ablation rate at fluences near threshold, as might be expected, even when the pulse width is up to ten times longer than the electron-lattice equilibration time.

In this paper we report experiments using intermediate duration pulses, 12-ps long, which show that in the same laser illumination conditions the ablation thresholds of metal targets irradiated in air are significantly lower than when the same targets are irradiated in vacuum. Analyzing this obser-

vation we found that the time to establish the high-energy tail of the Maxwellian energy distribution of atoms *at the surface* must be considered along with time for equilibration of the electron and lattice “temperatures.” Specifically, in vacuum the time needed to transfer energy from the high-energy Maxwellian tail from atoms in the bulk to the atomic layer at the surface (bulk-to-surface energy transfer time t_{b-s}) becomes the *crucial* parameter that determines the relative contribution of equilibrium (thermal) evaporation and nonthermal ablation to the material removal rate, especially near the ablation threshold. Our analysis, therefore, suggests that thermal ablation will only dominate when the pulse duration is comparable to or longer than the bulk-to-surface energy transfer time. The presence of air speeds up the creation of the Maxwellian distribution at the surface in effect increasing the role of thermal evaporation and leading to a reduction in the ablation threshold. Our results may be useful in explaining transition from short pulse to the long pulse ablation regime reported for different materials.^{1,2}

In this paper we first present experimental results on ablation of aluminum, copper, steel, and lead in air and in vacuum using 12-ps 532-nm pulses generated by a 50-W, 4.1 MHz mode-locked Nd:YVO₄ laser. We analyse the ablation mechanisms near and above the ablation threshold for these intermediate duration pulses. We demonstrate for the first time, to our knowledge, the importance of the time needed to transfer energy from the high-energy tail of the Maxwellian distribution created *in the bulk* to the nonequilibrium surface layer in laser ablation with short pulses. We develop a general theoretical model of laser ablation near and above the ablation threshold, based on the process of energy delivery to the atomic surface layer, and applied it to the ablation con-

ditions. The theoretical model is shown to be in good agreement with the experimental data.

II. EXPERIMENTAL RESULTS

A. Experimental conditions

The ablation experiments were carried out with laser pulses generated by a 50-W long-cavity mode-locked Nd:YVO₄ laser^{11,12} using a number of Al, Cu, steel (Fe), and Pb targets. The samples were exposed to 12-ps 532-nm pulses at a pulse repetition rate of 4.1 MHz; the energy per pulse on the target surface was $E_p=6.5 \mu\text{J}$. The beam profile measured after a multipass slab amplifier was close to a Gaussian shape with $M^2=1.15$ in the vertical direction and $M^2=1.4$ in the horizontal direction.¹²

Two sets of experiments were performed: one with the targets in air and the other in a vacuum of $\sim 5 \times 10^{-3}$ Torr. The energy per pulse and the pulse duration were fixed, while the energy density (fluence) was varied by moving the samples away from the focal plane of a 300-mm focusing lens so that the illuminated area was changed from $S_{f,\min}=4.9 \times 10^{-6} \text{ cm}^2$ ($d_f=25 \mu\text{m}$ FWHM) to $S_{f,\max}=1.2 \times 10^{-4} \text{ cm}^2$ ($d_f=124 \mu\text{m}$). This corresponded to a span of fluences from 5.4×10^{-2} to 1.3 J/cm^2 (or, of intensities from 4.2×10^9 to $1.0 \times 10^{11} \text{ W/cm}^2$). The profile of the focused beam was determined by attenuating the beam in front of the focussing lens and re-imaging the focal plane onto a CCD camera using a microscope objective. To avoid drilling craters in the target, the beam was scanned with X and Y oscillating mirrors operating at 61 and 59 Hz, respectively, over an area of approximately $17 \times 13 \text{ mm}^2$. This led to quasi-homogeneous scanning over the ablated area by creating a Lissajous scan pattern. The scanning speed is normally too slow to physically separate the beams from adjacent pulses for pulse trains in the 1–100 MHz range, many laser pulses still arrive at the same spot on the target surface. One can easily calculate the time that the laser beam “dwells” over a focal spot of size, d_f , for a given scanning frequency ω_s using the condition $\omega_s t_{\max}, \omega_s t_{\min} \ll 1$. Thus, the maximum dwell time is $t_{\max}=(4/\omega_s)(d_f/a)^{1/2}$. Similarly, the minimum dwell time near the center of a target at the maximum scanning velocity is $t_{\min}=d_f/a\omega_s$. In the conditions of our experiments $a \sim 15 \text{ mm}$, $d_f=25\text{--}124 \text{ microns}$, and $\omega_s \sim 60 \text{ s}^{-1}$. Therefore, the minimum and maximum dwell times are in a range $t_{\min}=2.8 \times 10^{-5}\text{--}1.38 \times 10^{-4} \text{ s}$, $t_{\max}=2.7 \times 10^{-3}\text{--}6 \times 10^{-3} \text{ s}$. Correspondingly, the minimum and maximum number of pulses hitting the same spot at 4.1 MHz repetition rate are $N_{\min}=115\text{--}566$, $N_{\max}=1.1 \times 10^4\text{--}2.48 \times 10^4$.

Since many pulses hit the same region of the target in succession, it is important to note that provided the target cools completely between consecutive pulses, then should be no interaction between them. The laser interaction with a target then proceeds in the same way as for a single pulse provided, of course, any crater formed by the preceding pulses is insignificant. This is the case near the ablation threshold. As will be shown later, the characteristic cooling time ($3 \times 10^{-11} \text{ s}\text{--}2 \times 10^{-10} \text{ s}$) for laser heated skin layer in the metals studied in these experiments is much shorter than the time gap between the pulses of $2.5 \times 10^{-7} \text{ s}$. Therefore,

target cools down completely between consecutive pulses and laser-target interaction near threshold proceeds in the single pulse mode.

It is important to achieve a high intensity contrast (the ratio between the peak pulse power to that of the background) during ablation experiments near the threshold to ensure that no surface modification occurs between the pulses due to, for example, amplified spontaneous emission. The energy contrast was measured at 1064 nm by using an acousto-optic modulator, triggered by the laser pulse train, as a gate to synchronously eliminate the mode-locked pulses from the output laser beam. This allowed the background power level between the pulses to be measured using a sensitive photodetector. Using the known pulse duration, the intensity contrast ratio R_c was found to be $R_c \approx 4 \times 10^7$. Since the output was frequency doubled in a nonlinear crystal the contrast ratio in the second harmonic beam should increase to $\approx R_c^2$ meaning that the emission between pulses was negligible. In addition five dichroic mirrors optimized for high 532-nm and low 1064-nm reflection were used to suppress the 1064-nm radiation at the target by a factor or $>10^7$.

B. Ablation mass, depth, and ablation thresholds

Total amount of material ablated over a 60-s period in the ablation experiments was measured by weighing the sample with the accuracy $\pm 10^{-4} \text{ g}$ before and after the ablation. The ablated mass per single pulse m_{av} was determined by averaging the mass difference over the 2.46×10^8 pulses. We introduce the ablation depth per single pulse as follows:

$$l_{\text{abl}} = \frac{m_{\text{av}}}{S_f \rho}, \quad (1)$$

where ρ is the target mass density and S_f is the focal spot area. To avoid redeposition of the ablated material back onto the target surface due to the collisions of the ablated vapors in the experiments in air, the vapors were sucked away from the target surface. The target has been examined after ablation under the optical microscope and no redeposition was found. If the redeposition did occur in a submicron scale, this would lead to an increase of the ablation threshold, while the experiments demonstrate the opposite. The measured ablation depths for various ablated materials as a function of the incident laser fluence are shown in Fig. 1.

There is an upper limit for the mass of material (or, maximum for the ablation depth) ablated by a single laser pulse with the pulse energy E_p (or fluence F_p), with atomic mass M_a and binding energy ε_b (energy of vaporization per atom) assuming total absorption, i.e., $A=1$. This is determined from energy conservation¹⁰

$$l_{\text{abl}}^{\max} = \frac{F_p M_a}{\varepsilon_b \rho}, \quad (2)$$

$$m_{\text{abl}}^{\max} = \frac{E_p M_a}{\varepsilon_b}. \quad (3)$$

The limiting values given by Eqs. (2) and (3) are higher than the experimental data. This indicates that the measured data

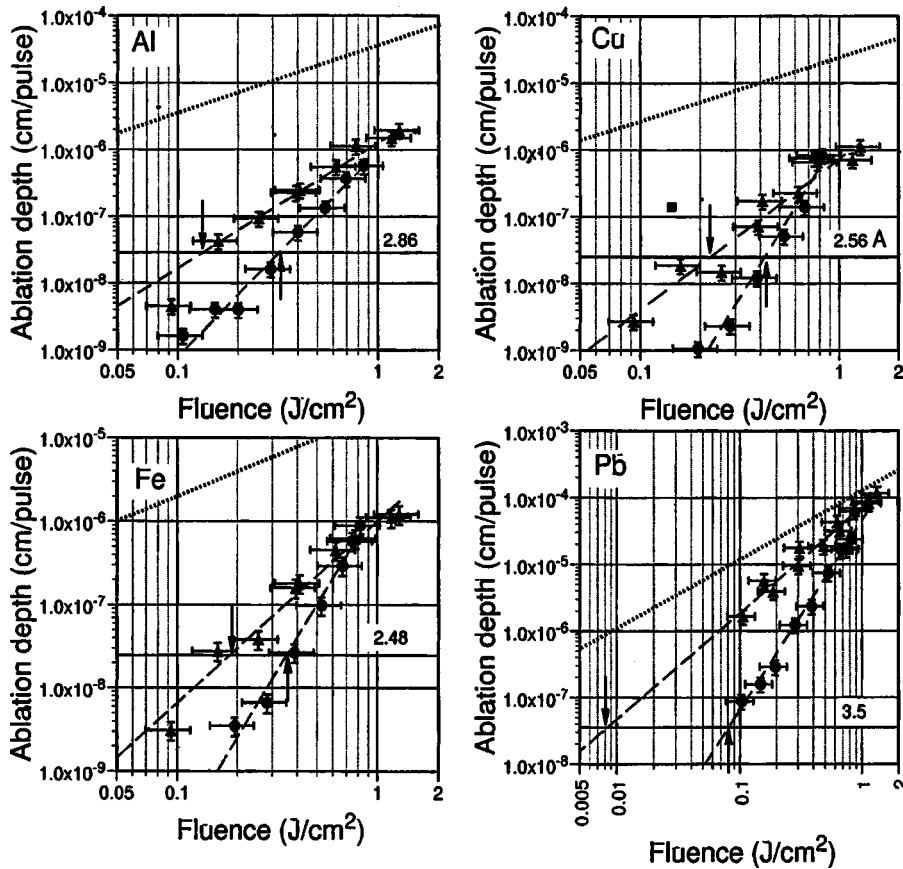


FIG. 1. Ablation depth per pulse vs fluence for (a) Al, (b) Cu, (c) Fe, and (d) Pb in experiments in air (triangles) and in vacuum (circles) using 12 ps 4.1 MHz repetition rate laser. The horizontal lines and the numbers above the lines correspond to interatomic distances (in angstroms), while the arrows indicate the ablation threshold. The dashed lines are the upper limits for the ablated depth determined using the energy conservation law.

are physically reasonable, and that the difference is caused by incomplete absorption A of laser radiation in the target ($A < 1$), energy loss to bulk heating of the target, and the energy expended in the form of kinetic energy of the expanding plume.

The measured ablation depth as a function of fluence allows one to determine the ablation threshold. The focal spot diameter is much larger than optical absorption depth, which is a few tens of nm corresponding to the skin depth of the metal. Thus, ablation can be considered as a one-dimensional process. The fluence at the ablation threshold can be determined by extrapolating the ablation depth dependence to the zero depth, such as it was used in a number of reports.^{2,3,6} However it appears that the threshold obtained this way may depend strongly on the extrapolation procedure since the fluence dependence is not a simple linear function. Indeed, it is known from statistical physics¹⁶ that the relative average fluctuation in the number of particles in an open system grows up as the average particles number goes to zero: $\sqrt{(\Delta N)^2}/N = 1/\sqrt{N}$. Therefore the relative error in experiments trying to measure the ablation threshold for a decreasing number of ablated atoms will increase. In practical terms repetition of an ablation experiment at the same fluence close to the ablation threshold should produce randomly scattered results in terms of particle removal. In our experimental data this is reflected by the fact that is impossible to find a physically justifiable extrapolation to zero depth. As a result it seems reasonable to define the ablation threshold as the energy density needed to remove a single atomic surface layer. The threshold introduced using this condition can be justified

by comparing the experimental and theoretical results for nonequilibrium ablation using femtosecond pulses.¹⁰ The ablation threshold fluence F_{thr} , derived in this manner from the experimental data for different metals is presented in Table I. We note that the threshold for Cu in vacuum, for example, of $0.41 \pm 0.05 \text{ J/cm}^2$ is in good agreement with the results of Nolte *et al.*³ ($F_{thr} = 0.375 \text{ J/cm}^2$ for 9.6-ps and 0.423 J/cm^2 for 14.4-ps pulses).

Table I shows that for all the metals studied the ablation threshold in air was found to be noticeably lower than in vacuum. We emphasize that these experiments were carried out using identical laser and focusing conditions so that the only significant variable was the presence or absence of air. Hence the errors in the relative values presented in Table I are small.

In what follows we consider below the physical processes during the pulse and after the end of the pulse in order to understand why air should influence the ablation rate and threshold. In particular we search for the explanation of why the ablation depth in air near threshold is much larger than

TABLE I. Threshold fluence for ablation of metals by 12-ps pulses measured in air and in vacuum.

Metal, M_a [a.u.]	Al, 26.98	Cu, 63.54	Fe, 55.85	Pb, 207.19
F_{thr} in air, [J/cm ²]	0.17 ± 0.03	0.23 ± 0.03	0.19 ± 0.02	0.008 ± 0.002
F_{thr} in vacuum, [J/cm ²]	0.32 ± 0.04	0.41 ± 0.05	0.36 ± 0.04	0.08 ± 0.02

TABLE II. Plasma frequency, time for the energy transfer from electrons to the lattice, and thermal diffusion rate calculated with the electron effective masses (Refs. 14 and 30) (see details in Appendix B).

Metal	Al	Cu	Fe	Pb
$\omega_{pe} = (4\pi e^2 n_e / m_e)^{1/2}$, 10^{16} s ⁻¹	1.97	1.395	0.82	1.46
t_{ei} (ps)	1.695	6.04	1.55	13.2
t_{th} (ps)	26.2	25.6	96.0	139.6
C_e (in units k_B)	0.473	0.76	0.122	0.269

when the same target is irradiated in the same conditions in vacuum. We also discuss a difference between the single-pulse and the multiple-pulse laser ablation which could be relevant to the conditions of these experiments.

III. DISCUSSION

Two qualitatively different ablation mechanisms must be considered for the intermediate range pulse duration used in these experiments: one is nonthermal ablation and the other is thermal evaporation. Nonthermal ablation occurs when the surface atoms gain an average energy (T) from the laser greater or equal to the binding energy ε_b . In such conditions atoms from the outermost surface layer can leave the surface with kinetic energy equal to $T - \varepsilon_b$. Note that nonthermal ablation ceases to exist when $T < \varepsilon_b$. In such conditions only thermal ablation occurs which involves the escape of atoms whose energy exceeds ε_b from the high-energy tail of the Maxwellian distribution.

The processes of laser energy absorption by electrons, energy transfer from electrons to ions, and the establishment of the Maxwellian energy distribution among the atoms takes place both during and after the laser pulse. The contribution of thermal evaporation and nonthermal ablation to the total material removed from the surface essentially depends on the duration of these energy transfer processes. In what follows we estimate the characteristic times of these processes and calculate the ablation thresholds for ablation in vacuum and in air by a single pulse comparing the result to those of our experiments.

A. Electron-to-ion energy-transfer time

First, let us consider the electron-ion collision frequency in the absorbing layer. The maximum electron temperature in this surface layer rises up to a few eV by the end of the laser pulse. The effective electron-ion collision frequency ν_{ei} for momentum transfer is of the order of magnitude of the electron plasma frequency ω_{pe} : $\nu_{ei} \cong \omega_{pe}$.⁹ The time for energy transfer from electrons to ions is expressed as $t_{energy} = (\nu_{ei} m_e / m_i)^{-1}$. This time for the metal targets used in the experiments is shown in Table II. It is evident that in all metals except Pb almost all the absorbed laser energy is already transferred to the ions by the end of the 12-ps pulse. The thermal diffusion rate $t_{th} = l_s^2 / D$, is also shown for comparison in Table II, to demonstrate that thermal diffusion from the absorbing skin layer occurs much more slowly. We

note here that the electron-ion energy exchange time is close to the electron-phonon coupling time (see Appendix A). These data are in a good fit to the data known from the literature.¹⁻¹⁰

B. Temperature in the skin layer during the pulse

The characteristic heat conduction time in metals, which is $t_{th} \cong l_s^2 / D$, is at least a few times longer than the 12-ps laser pulse (D is the thermal diffusivity presented in Appendix B). Therefore, any heat wave propagates to a distance less than the skin depth during the pulse. For this reason we can neglect heat conduction from the calculations of the maximum temperature to the pulse end in the surface layer.^{2,10} Then the temperature in the skin layer during a single laser pulse can be calculated using a two-temperature approximation¹³

$$C_e n_e \frac{\partial T_e}{\partial t} = \frac{2A}{l_s} I(t) - \frac{n_e}{t_{eL}} (T_e - T_L),$$

$$C_L n_a \frac{\partial T_L}{\partial t} = \frac{n_e}{t_{eL}} (T_e - T_L), \quad (4)$$

where n_e and n_a are, respectively, the electron and the atomic number density, C_e and C_L are the heat capacity of the electrons and of the atoms in the lattice, A is the absorption coefficient, $l_s = c / \omega \kappa$ is the skin depth (ω is the laser light frequency, κ is the imaginary part of the refractive index, and c is the speed of light in vacuum), and $I(t)$ is the laser pulse intensity. The pulse has the Gaussian time shape $I(t) = I_0 \exp[-\pi(t/t_p - 1)^2]$. Correspondingly the total fluence to the end of the pulse is then expressed as $F = I_0 t_p (1/\sqrt{\pi} + 1/2) = 1.064 I_0 t_p$.

Special note should be made of the specific heat (the heat capacity) of the electrons and the lattice in metals. The conductivity electrons in metals are degenerate if the temperature is lower than the corresponding Fermi energy ($T_e < \varepsilon_F$). The Fermi energy is usually higher than the binding energy for the metals. Therefore, the electrons are degenerate below and near the ablation threshold. The specific heat of degenerate electrons is conventionally expressed as follows:¹⁴

$$C_e \approx \frac{\pi^2 k_B T_e}{2 \varepsilon_F}. \quad (5)$$

The specific heat for atoms is equal to $3k_B$ per atom at low temperature when the atomic motion has an oscillatory character. At higher temperature the vibrational motion of atoms changes to a translational one as for a monoatomic gas. The atom specific heat gradually decreases to the level of $3k_B/2$ per atom with increasing temperature. The effective boundary dividing the temperature ranges, where the two limiting values of the atomic specific heat are valid, can be associated with a potential barrier against the free motion of atoms through the solid. The temperature T_b at the potential barrier is related to the binding energy $T_b \sim 2\varepsilon_b/3$.¹⁵ Thus, the increase in lattice temperature as the ablation threshold is approached is accompanied by a change in the specific heat of the atoms.

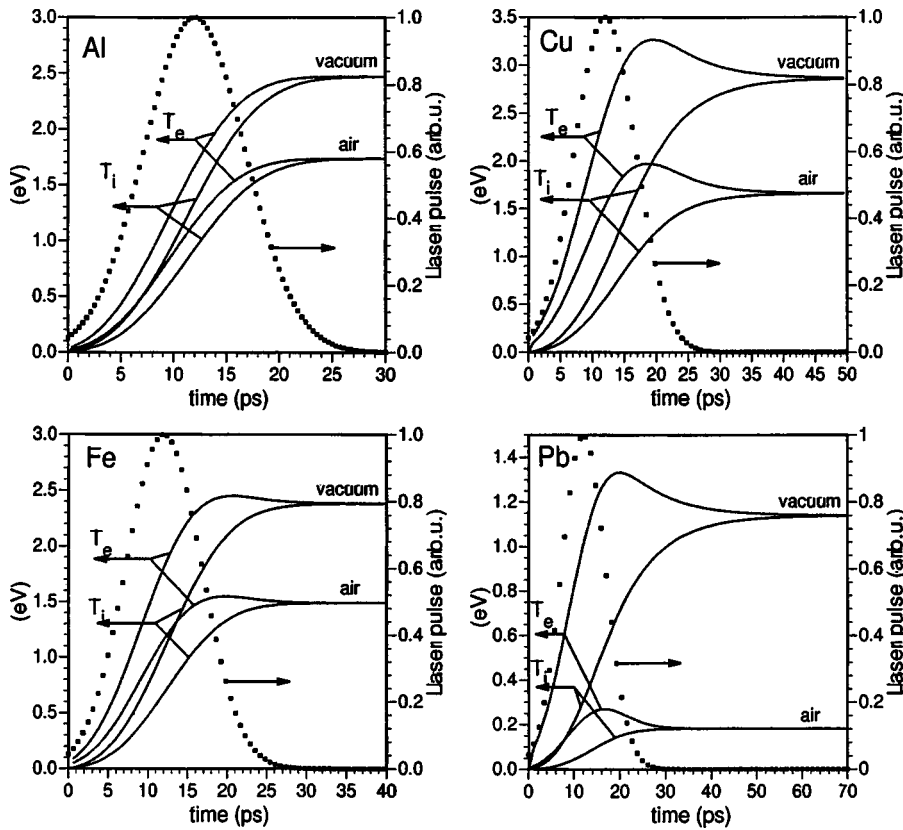


FIG. 2. Calculated electron and lattice temperature in the skin-layer at the ablation threshold in Al, Cu, Fe, and Pb in vacuum and in air, together with the Gaussian profile of the 12-ps laser pulse.

The electron and lattice temperatures in the surface layer at the ablation threshold in vacuum for each metal can be calculated taking the experimentally determined threshold fluence from Table I, and “hot” plasma optical parameters from Appendix A. The results of numerical calculations of Eq. (4) are presented in Fig. 2, and the maximum temperature at the end of the laser pulse in air and in vacuum are presented in Table III.

It can be seen from the results that the maximum surface temperature in vacuum is close to the binding energy, thus we can conclude that ablation of metals in vacuum at the ablation threshold starts as a nonequilibrium process. However, the ablation in air starts at a temperature about half the binding energy for Al, Cu, Fe, and 10 times lower for Pb. This is a clear indication of the dominance of the thermal mechanism of evaporation in air. In order to understand the difference we shall analyze the energy transfer from the bulk of the heated material to the outermost atomic surface layer where removal of atoms begins. It is also instructive to revisit the conditions and the formulae for conventional evaporation in thermodynamic equilibrium, and compare them to the conditions during and after the pulse.

TABLE III. Maximum surface layer temperature at the ablation threshold fluence in vacuum and in air. The binding energies are presented for comparison.

	Al	Cu	Fe	Pb
T_{\max} , eV (vacuum)	2.5	2.9	2.39	1.15
T_{\max} , eV (air)	1.74	1.66	1.49	0.18
Binding energy ε_b , eV	3.065	3.125	3.695	1.795

C. Thermal evaporation in equilibrium conditions

1. Saturated pressure

The pressure at a solid-vapor boundary in equilibrium conditions (the saturated pressure) is defined by the condition that the pressure, temperature, and chemical potential for both equilibrated phase states coincide at the interface¹⁶

$$P = \text{const} \times T^{c_p - c_s} \exp\{-\varepsilon_b/T\}, \quad (6)$$

where c_p is a specific heat at a constant pressure for the vapor, $c_p = 5/2 k_B$ (for monoatomic gas), $3/2 k_B \leq c_s \leq 3 k_B$ is the specific heat for a solid, depending on density, and ε_b is the heat of evaporation per atom or the binding energy. In conditions close to the critical point one can take $c_p - c_s \cong k_B$.

2. Thermal ablation rate

In equilibrium conditions at the solid-vapor interface the number of particles leaving the solid per unit time from the unit area equals to the number of particles coming back from the vapor. The differential collision rate for the atoms in the vapor with the solid surface, in atoms/cm²s, is

$$dv = v dn_a, \quad (7)$$

where v is the atom thermal velocity and n_a is the vapor number density. Integration of Eq. (7) with the Maxwellian distribution

$$dn_a = n_a \left(\frac{M_a}{2\pi T} \right)^{3/2} \exp\left(-\frac{M_a v^2}{2T}\right) 4\pi v^2 dv$$

produces the evaporation rate as follows:¹⁶

$$\nu \equiv (n_a v)_{\text{therm}} = \frac{n_a T}{(2\pi M_a T)^{1/2}} = \frac{P}{(2\pi M_a T)^{1/2}}, \quad (8)$$

where M_a is the atomic mass and P is the pressure of saturated vapor defined by Eq. (6). The density of the saturated vapor in equilibrium n_a is expressed in the form

$$n_a = \text{const} \times T^{c_p - c_s - 1} \exp\left\{-\frac{\varepsilon_b}{T}\right\} \propto \exp\left\{-\frac{\varepsilon_b}{T}\right\}. \quad (9)$$

Equilibrium evaporation in vacuum is conventionally considered as evaporation at the saturated vapor density corresponding to the equilibrium temperature.¹⁶ However, one should exercise caution with a direct application of the above equilibrium evaporation formulas to nonequilibrium ablation by short laser pulses. These equilibrium formulas, as we demonstrate below, can only be applied *after* the time needed to establish both the main part *as well as the high-energy tail* of the Maxwellian energy distribution.

D. Time to establish the Maxwellian energy distribution

We estimate the time needed to establish a Maxwellian distribution in the skin layer at temperature near $(1/3 - 1/2)\varepsilon_b$, close to the experimentally observed ablation threshold in air. The atom-atom collision time in a neutral solid is conventionally estimated as $t_{\text{coll}} \cong (n_a \sigma_0 v)^{-1} \cong (5 \times 10^{22} \text{ cm}^{-3} \times 5 \times 10^{-16} \text{ cm}^2 \times 3 \times 10^4 \text{ cm/s})^{-1} \cong 10^{-12} \text{ s}$ (here $\sigma_0 = \pi r_0^2$ is the cross section for atomic collisions and r_0 is the atomic radius). Alternatively in a heated solid density plasma the time for Coulomb collisions reads $t_{\text{coll-p}} \sim (n \sigma_p v)^{-1} \sim T^{3/2}$.¹⁷ Both these times correspond to that required to establish the main part of the Maxwellian distribution $t_{\text{coll}} \sim t_{\text{main}}$. However, it was found a long time ago that the time needed to establish the *high-energy tail* of the equilibrium distribution in plasma is much longer than this collision time.¹⁸ In a plasma the time to establish the high-energy tail can be estimated for a particular energy $\varepsilon \gg T$, as $t_{\text{tail}} \approx t_{\text{main}} (\varepsilon/T)^{3/2} \gg t_{\text{main}}$.

In the conditions of our experiments the temperature is of the order of an electronvolt. At the temperature of 1 eV the degree of ionization is only $\sim 10\%$, therefore we shall estimate the time to create the high-energy tail in a neutral solid in conditions where $T_{\text{melt}} \ll T \ll \varepsilon_b$. The solid is in a disordered state at $T \gg T_{\text{melt}}$. Thus the interatomic energy exchange occurs due to random collisions. In order to increase the energy of an atom from T to ε_b , the atom should experience $N = \varepsilon_b / \Delta T$ isotropic and statistically independent collisions, each of which increases the atom's energy from T to $T + \Delta T$ ($\Delta T = T/n \ll T$, $n \gg 1$). The probability of such energy increase is expressed as follows:

$$W(T \rightarrow \varepsilon_b) = \left(\frac{T}{T + \Delta T}\right)^N = \left(\frac{1}{1 + n^{-1}}\right)^{n(\varepsilon_b/T)}. \quad (10)$$

In the limit of $n \gg 1$, e.g., taking into account that $\lim_{n \rightarrow \infty} (1 + n^{-1})^n = e$, the above formula attains the recognizable equilibrium features

$$W(T \rightarrow \varepsilon_b) = e^{-\varepsilon_b/T}. \quad (11)$$

Now, the cross section to reach energy ε_b in the conditions $T \ll \varepsilon_b$ takes the following form:

$$\sigma_{T \rightarrow \varepsilon_b} = \sigma_0 W(T \rightarrow \varepsilon_b) = \sigma_0 e^{-\varepsilon_b/T}. \quad (12)$$

The time to establish the high-energy tail in isotropic conditions characteristic of a bulk solid which has undergone an instantaneous rise of temperature to $T \ll \varepsilon_b$ then reads

$$t_{\text{tail}} = t_{\text{main}} e^{\varepsilon_b/T}. \quad (13)$$

Taking, for example, the average temperature in the skin layer of ~ 1 eV, which is close to the threshold conditions with 12-ps pulses, and the binding energy of ~ 3 eV, the high-energy Maxwellian tail is established in the bulk in a time of about $10 t_{\text{main}} \sim 2$ ps (taking $t_{\text{main}} \sim 0.2$ ps).

The question that now arises is whether the time to create the Maxwellian distribution in the bulk also applies to the surface layer. The atoms in the outermost surface layer next to the vacuum are in fact in a different condition compared to the atoms in the bulk. Below we consider the processes responsible for the removal of instantaneously heated atoms from the surface layer into vacuum, and consider relative contribution from thermal and nonthermal processes of ablation of atoms near the ablation threshold.

E. Time for the energy transfer from the bulk to the outermost surface layer

It is well known that the surface atoms are loosely bound to the bulk making part of bonds dangling or saturated with foreign atoms.^{19,20} The effects of different bonds leads to decreases in the Debye and melting temperatures, to changes in the bond length and interatomic distance as well as the crystalline structure, and the nature and rate of any phase transition. However, as was noticed by Prutton:¹⁹ "...many surface phases are actually metastable, i.e., the surface is not in a true thermodynamic equilibrium." The energy distribution in the outermost surface layer is the important characteristic affecting the removal of atoms from the surface layer at the ablation threshold. The energy distribution is responsible for the relative contribution of nonequilibrium ablation and thermal evaporation.

Atoms from the outermost surface layer will immediately leave a solid if energy in excess of binding energy is instantaneously deposited into this layer. This is the process of nonequilibrium ablation.¹⁰ In equilibrium conditions, the evaporation can proceed at a much lower temperature than the binding energy. This is due to the existence of high-energy atoms in the Maxwellian tail with $\varepsilon \geq \varepsilon_b$. However, the presence of the free surface prevents the equilibrium from being established in the surface layer itself whose thickness is comparable to the mean free path for atomic collision. This thickness is close to the thickness of a monoatomic layer. Indeed, if the energy of an atom in this layer reaches the binding energy due to collisions with the atoms from the bulk, this atom immediately escapes from the solid. Thermal evaporation from the surface heated to a temperature below the binding energy can therefore, only proceed

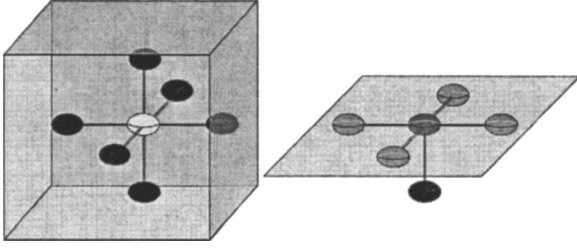


FIG. 3. Close neighbor atoms (colored black) delivering high energy by collisions in a bulk (left) and at the surface (right).

when energy is supplied to the surface from the bulk via atom-atom collisions. Thus, the time for the energy to increase from $\varepsilon = T < \varepsilon_b$ to $\varepsilon \geq \varepsilon_b$ in the surface layer (that is the bulk-to-surface energy transfer time t_{b-s}) determines the onset of the thermal evaporation at solid-vacuum interface. This time is analogous to the time needed to establish the Maxwellian tail in isotropic conditions in the bulk. The probability of energy transfer from the bulk to the surface can be found from a solution of the time-dependent two-dimensional kinetic equation, which is a formidable problem! However, one can make a reasonable estimate as follows.

It is clear that the probability of energy transfer in excess of ε_b from atoms in the bulk to those at the surface should be lower than that between atoms in the bulk due to a decrease in the number of close neighbors around the surface atom capable of such energy transfer. For example, the number of close neighbors (n_b) equals 6 in the bulk of a closely packed solid whereas the number of close neighbors from the bulk (n_s) for a surface atom is only 1 because the other four closest neighbors are also surface atoms (see Fig. 3). Therefore the number of collisions required to increase the energy of a surface atom N_{surf} will need to be larger compared to that in the bulk $N_{\text{surf}} \sim b \times N_{\text{bulk}}$, where $b \approx n_b/n_s$. Correspondingly, the probability of energy transfer from the bulk to the surface should be lower in accordance with Eq. (10): $W_{\text{bulk}} \sim W_{\text{surf}}^{N_{\text{bulk}}}$, $W_{b-s} \sim W_{\text{surf}}^{N_{\text{surf}}} \sim W_{\text{bulk}}^b$. Then the cross section for a collision between atoms in the bulk with the surface atoms can be presented in the form

$$\sigma_{b-s} = \sigma_0 W_{b-s} \sim \sigma_0 W_{\text{bulk}}^b. \quad (14)$$

Now one can arrive to the following estimate for the cross section for the bulk-to-surface energy transfer

$$\sigma_{b-s} \approx \sigma_0 W_{b-s}(T \rightarrow \varepsilon_b) \approx \sigma_0 e^{-b(\varepsilon_b/T)}. \quad (15)$$

The bulk-to-surface energy transfer time thus reads

$$t_{b-s} = [n_a v \sigma_{b-s}]^{-1} \approx t_{\text{main}} e^{b(\varepsilon_b/T)}. \quad (16)$$

According to Eq. (16), the bulk-to-surface energy transfer time increases dramatically with decreasing temperature. For example at $T \sim \varepsilon_b/2$, $t_{b-s} \approx 1.6 \times 10^5 t_{\text{main}} \sim 3 \times 10^4$ ps. Hence one can see that the bulk-to-surface energy transfer time exceeds markedly the electron-to-lattice thermalization time and the heat conduction time at fluences that are below the threshold for nonthermal ablation. In other words as the surface starts to cool by thermal conduction, the bulk-to-surface energy transfer time increases to such an extent that it makes

it impossible for the surface atoms to gain energy above the binding energy. Hence thermal evaporation does not occur.

F. Contribution of thermal evaporation at $t > t_{b-s}$

The total ablation is the sum of contributions from non-equilibrium mechanism at $t < t_{b-s}$ and thermal ablation at $t > t_{b-s}$ if the threshold condition for the nonthermal ablation in vacuum is achieved. To quantify this process, let us consider the relative contribution from thermal and nonthermal ablation mechanisms in vacuum when the nonthermal threshold condition is achieved. The outermost atomic layer, where $T_{\text{max}} \sim \varepsilon_b$, is removed, thus the ablation depth equals the interatomic distance d . Thermal ablation starts after a time t_{b-s} when the energy in excess of the binding energy is delivered to the surface layer from the bulk through atomic collisions. The depth of material removed by thermal evaporation can be expressed through the time- and space-dependent distribution function as follows:

$$l_{\text{th}} = \frac{1}{n_a} \int_{t_{b-s}}^{\infty} \int_0^{\infty} \bar{v} f(\bar{v}, t) d^3 \bar{v} dt. \quad (17)$$

The transient distribution function differs from the equilibrium one only by the high-energy tail. Therefore, the average density $n_a = \int f(\bar{v}, t) d^3 \bar{v}$ and the average velocity $v[T(t)] = \int \bar{v} f(\bar{v}, t) d^3 \bar{v}$ are close to their equilibrium values. The number density of evaporating atoms (analogous to the saturated density of vapor in equilibrium) can be approximated as $n \approx n_a \exp[-b(\varepsilon_b/T)]$. Then the evaporation depth in Eq. (17) is expressed as

$$l_{\text{th}} \approx \int_{t_{b-s}}^{\infty} \left(\frac{2T}{M} \right)^{1/2} e^{-b(\varepsilon_b/T)} dt. \quad (18)$$

The temperature decreases in accordance with linear heat conduction $T = T_{b-s}(t_{b-s}/t)^{1/2}$, $T_{b-s} \equiv T(t_{b-s})$. The latter is expressed as follows:

$$T_{bs} = T_m \left(\frac{t_{\text{th}}}{t_{\text{th}} + t_{b-s}} \right)^{1/2}. \quad (19)$$

Then, Eq. (18) can be immediately integrated to obtain (see Appendix C):

$$l_{\text{th}} \approx t_{b-s} \left(\frac{2T_{bs}}{M} \right)^{1/2} \frac{T_{bs}}{2\varepsilon_b} e^{-b\varepsilon_b/T_{bs}}. \quad (20)$$

The maximum temperature at the end of the pulse in the absence of losses is proportional to the total absorbed fluence $T_m \sim F_a$.¹⁰ Hence the thermal evaporation depth scales with the absorbed fluence as $l_{\text{th}} \approx F_a^{3/2}$.

A conservative estimate taking the maximum surface temperature at the nonthermal ablation threshold $T_m \sim \varepsilon_b$, $t_{b-s} \sim 80$ ps, $t_{\text{th}} \sim 30$ ps, $v \sim 10^5$ cm/s, $T_{bs} = 0.52 T_m$ gives $l_{\text{th}} \sim 2 \times 10^{-11}$ cm $\ll d_a$. Thus, nonequilibrium ablation completely dominates thermal evaporation. We therefore can conclude that in vacuum thermal evaporation at the ablation threshold and below that threshold is completely negligible.

TABLE IV. Threshold fluence for ablation of metals by 532 nm 12-ps pulses calculated assuming plasma conditions compared with those measured in the experiments in air and in vacuum.

Metal	Al	Cu	Fe	Pb
$F_{\text{thr}}[\text{J}/\text{cm}^2]$, Eq. (21)	0.34	0.404	0.28	0.106
F_{thr} in vacuum, [J/cm ²]	0.32±0.04	0.41±0.05	0.36±0.04	0.08±0.02
F_{thr} in air, [J/cm ²]	0.17±0.03	0.23±0.03	0.19±0.02	0.008±0.002

G. Ablation threshold in vacuum

From the above we have concluded that the ablation of metals in the experiments in vacuum is essentially a nonthermal process. The threshold laser fluence can be defined from the condition that the temperature at the end of the pulse equals to the binding energy¹⁰

$$F_{\text{th}}^m \approx \frac{l_s \varepsilon_b}{2A} \{C_e(\varepsilon_b) n_e + 1.5 n_d\}. \quad (21)$$

We note that the above threshold definition is based on the calculation of temperature under the assumption that all the losses are negligible.

In the long pulse limit electron thermal conduction determines the depth of the zone where the energy is deposited $l_{\text{th}} \gg l_s$. Equation (21) then reproduces the well-known square-root dependence on the pulse duration since the skin length is replaced by the heat conduction length $l_{\text{th}} = (Dt_p)^{1/2}$.^{21,22} This dependence of the ablation threshold on the laser fluence would be expected to start at pulse durations for which thermal losses become significant during the laser pulse.

Finally we refine our estimate of the ablation threshold in the resulting nonthermal conditions in vacuum. To make such estimates we need reliable values for the optical parameters of the surface. The optical parameters of metals at room temperature are well documented²³ (see also Appendix A). However, atoms in the surface skin layer are partially ionized at the temperatures near the ablation threshold, hence the optical properties such as absorption, skin depth, can change, and are difficult to measure during and after the laser pulse.^{24,25} We, therefore, calculate these optical properties assuming the existence of hot plasma in the surface layer (see Appendix A). These calculations are in agreement with more complicated computer simulations,²⁶ which take into account two-temperature hydrodynamics and transient absorption changing from the cold metal to plasma during the laser pulse. The calculated ablation thresholds for a single 12-ps laser pulse ($\lambda = 532$ nm) are presented in Table IV. The calculated threshold values are in reasonably close agreement with the experimental data in vacuum. However, the most significant differences exist between the ablation thresholds in air and in vacuum. In order to understand these differences we shall consider how the presence of air can effect thermal evaporation that is the only process that can occur below the vacuum ablation threshold. The question is

how is thermal evaporation “turned on” by the presence of air when we concluded it is negligible in vacuum?

H. Thermal ablation in air after the pulse

Before we can proceed to analyze ablation in air, we have to be sure that there is no optical breakdown in the air next to the surface in the conditions of the experiments. Breakdown of air by 10 ps pulses produced by a Nd:YAG laser (1064 nm) has been reported to occur at an intensity of 3×10^{14} W/cm².²⁷ The breakdown time scales in inverse proportion to $\propto (I \times \lambda^2)^{-1}$, thus the breakdown threshold for 12-ps 532-nm laser should be around 10^{15} W/cm². The maximum intensity in our experiments was of the order of 10^{11} W/cm², which appears well below the expected breakdown threshold. Indeed, no breakdown (no spark) was observed, therefore we can conclude that the vapors remained neutral during the experiments.

After the laser pulse, the air next to the heated surface layer gains energy through collisions with the solid target. This results in the establishment of a Maxwellian distribution in the air near the air-solid interface. Hence it is possible for the air to play the same role as the saturated vapor in classical thermal evaporation. The presence of air introduces a new pathway allowing the creation of the high-energy tail of the Maxwellian distribution in the surface layer augmenting the bulk-to-surface energy transfer process discussed earlier. Thus there are now three processes acting at the same time which determine the ablation conditions at the solid-air interface: (i) evolution of the Maxwellian distribution at the surface due to air-solid collisions, (ii) evolution of the Maxwellian distribution at the surface due to bulk-to-surface energy transfer, and (iii) cooling of the surface layer by heat conduction. Whereas we concluded that mechanism (ii) was too slow to result in thermal evaporation when $T < \varepsilon_b$ the role of the air could be to significantly increase thermalization at the surface allowing thermal evaporation to take place after the air-solid equilibrium has become established. The ablation rate then can be calculated using thermodynamic phase equilibrium relations, which link the saturated vapor density (pressure) to the vapor temperature. Let us consider all these processes in sequence.

The air-solid equilibrium energy distribution is established by collisions of air molecules with the solid. The gas-kinetic mean free path in air in standard conditions is $l_{g-k} = 6 \times 10^{-6}$ cm.¹⁵ Therefore, the equilibration time t_{eq} needed to establish a Maxwellian distribution in the gas can be estimated as $t_{\text{eq}} \sim l_{g-k}/v_{\text{th}}$, where v_{th} is the average thermal velocity in air. We estimate this time at room temperature ($v_{\text{th}} = 3.3 \times 10^4$ cm/s) $t_{\text{eq}} \sim 1.8 \times 10^{-10}$ s. The bulk-to-surface energy transfer time calculated by Eq. (16) at the maximum temperature ($T_{\text{max}} \sim \varepsilon_b/2$) for conditions equal to the threshold fluence in air constitutes $t_{b-s} \approx t_{\text{main}} e^{12} \sim 30 \text{ ns} \gg t_{\text{eq}}$ for Cu, Al, and Fe after the pulse. Thus, only the air-surface collisions could lead to the formation of high-energy Maxwellian tail, and therefore to thermal evaporation from the surface.

The evaporation rate can be calculated in the following way. The solid-air temperature equilibration is completed

when the surface temperature has dropped due to thermal conduction to $T_{\text{eq}}=T_m(t_p/t_{\text{eq}})^{1/2}$. Here T_m is the maximum temperature at the end of the laser pulse at the experimental-determined threshold fluence for ablation in air. The values were presented in Table III. Thermal evaporation starts after the equilibration time $t > t_{\text{eq}}$ and the temperature at the solid-air surface continues to decrease in accordance to the linear heat conduction law. We suggest that thermal evaporation proceeds at a vapor density corresponding to the temperature at the solid-air interface. The number of atoms ablated per unit area after establishing the Maxwellian equilibrium can be estimated as

$$\langle nvt \rangle_{\text{therm}} = \int_{t_{\text{eq}}}^{\infty} (nv)_{\text{therm}} dt. \quad (22)$$

A reliable estimate of the evaporation rate can be obtained with the numerical coefficients extracted from the known experimental data at the temperature close to our experimental conditions. Such data exist for copper: at the temperature $T=0.25$ eV ($\cong 2850$ K) the saturated vapor pressure and density are, respectively, 10^7 erg/cm³ and 2.67×10^{19} cm⁻³.²⁸ With the help of Eq. (9) the interpolation formula for the ablation rate then follows:

$$(nv)_{\text{th,Cu}} = 8.95 \times 10^{31} \exp \left\{ -\frac{4.85}{T[\text{eV}]} \right\} \left[\frac{\text{atoms}}{\text{cm}^2 \text{ s}} \right]. \quad (23)$$

Integration of Eq. (22) with Eq. (23) and $T=T_m(t_p/t)^{1/2}$ results in the ablation rate of 5.28×10^{15} cm⁻². Another interpolation for the saturated vapor density:²⁸

$$n_{\text{sat,Cu}} = 2.67 \times 10^{19} \exp \left[-\frac{3.173(4T[\text{eV}] - 1)}{T[\text{eV}]} \right]$$

yields an ablation rate of 4.26×10^{15} cm⁻², which is very close to that from the interpolation by Eq. (23).

Unfortunately we could not find any high temperature data for Al, Fe, and Pb. However, thermal ablation rates can be estimated assuming that the equilibrium in the vapor-air mixture with a predominance of air plays a role of the saturated vapor over the ablated solid. Then one can estimate Eq. (22) as

$$\langle nvt \rangle_{\text{therm}} = \int_{t_{\text{eq}}}^{\infty} (nv)_{\text{therm}} dt \approx \frac{n_{\text{air}} T_{\text{eq}}^{1/2}}{(2\pi M_a)^{1/2} t_{\text{eq}}} \left[\frac{\text{atoms}}{\text{cm}^2} \right]. \quad (24)$$

The resulting values should be compared to the corresponding areal number density $n_a \times d_{\text{mono}}$ in the atomic monolayer which corresponds to our threshold condition as described earlier. The values predicted by Eqs. (23) and (24) are presented in Table V for comparison with the areal density of a monolayer. It is clear that the predicted number of the thermally ablated atoms is, in fact, close to the number of atoms in a monoatomic layer.

Table V suggests that thermal evaporation well after the end of the laser pulse at fluences corresponding to the threshold measured in air can, indeed, be responsible for the removal of a monoatomic layer for Al, Cu, and Fe. This is in a good agreement with the experiments, as the threshold fluence was introduced as the fluence needed to remove a single

TABLE V. The predicted numbers of atoms thermally evaporated after the pulse once a Maxwellian distribution has been established compared with the number of atoms in a monolayer.

	Al	Cu	Fe	Pb
$[nvt]_{\text{therm}}, 10^{15} \text{ cm}^{-2}$, Eq. (24)	2.4	5.28	1.67	0.45
$[nvt]_{\text{therm}}, 10^{15} \text{ cm}^{-2}$, Eq. (23)		4.26		
$n_a \times d_{\text{mono}}, 10^{15} \text{ cm}^{-2}$ (number of atoms in a monolayer)	1.72	2.16	2.0	1.15

atomic layer. Therefore, we can conclude that the presence of air *decreases* the single pulse ablation threshold by approximately a factor of two relative to the vacuum case due to the contribution of thermal ablation assisted by the presence of the air well after the end of the pulse.

The measured ablation thresholds for Pb in air and in vacuum differed by an order of magnitude and the calculated results for lead are somewhat lower relative to the areal density of a monolayer than for the other materials. It should be noted that this may be caused by the fact that the optical properties of lead as function of temperature are poorly known and could differ from the ‘‘hot’’ plasma parameters used in this paper (Appendix A). It is also possible that Pb has a more pronounced cumulative effect from consecutive pulses (as will be discussed next). As one can see from Eq. (21), the ablation threshold is a function of absorption coefficient, which is temperature dependent. For example, the use of optical characteristics for cold aluminium can lead to an order of magnitude difference in the expected ablation threshold.

I. Multipulse thermal ablation in vacuum

As demonstrated in the previous section, the presence of a gas next to the solid surface increases the ablation rate due to thermal evaporation after the pulse. A similar effect may take place when a high repetition rate laser is used for ablation because of the accumulation of a dense vapor in front of the solid target surface from successive pulses.

One can estimate the conditions for such accumulation effects as follows. Thermal ablation can be efficient once a Maxwellian distribution between the vapor and the solid has been established. Thus, the first condition for cumulative evaporation is that the equilibration time should be shorter than the time gap between the pulses $t_{\text{eq}}=(n\sigma v)^{-1} < R_{\text{rep}}^{-1}$. From this condition, the vapor density should comply with condition $n > (R_{\text{rep}}/\sigma v)$. Thus, taking the experimental conditions $R_{\text{rep}}=4.1 \times 10^6 \text{ s}^{-1}$, $\sigma \sim 10^{-15} \text{ cm}^2$, and $v_{\text{th}} \sim 10^5 \text{ cm/s}$, the vapor density should be $n_a > 4 \times 10^{16} \text{ cm}^{-3}$. Thus, for the vacuum ablation in our experiments at $P=3 \times 10^{-3} \text{ Torr}$ ($n_a=1.8 \times 10^{14} \text{ cm}^{-3}$) the density near the ablated surface should increase more than 200 times due to the action of many consecutive pulses.

Let us consider the conditions for such density build up. The plume expands adiabatically because the entropy and the energy are conserved after the pulse. The specific features of the isentropic expansion are the follows: the density and the temperature of a plume go to zero at the finite distance from

the initial position (in contrast to isothermal expansion), while the velocity is at maximum.¹⁵ Therefore the density next to ablation surface has a steep gradient. The size of the expanding plume grows linearly with time:

$$R_{\max} = \frac{v_{\text{th}}}{R_{\text{rep}}}, \quad (25)$$

which is ~ 250 microns in experiments. The experimental data of Fig. 1 indicate that slow nonequilibrium ablation does take place when the surface temperature is as little as half the ablation threshold. This is plausible because only a few collisions can lead to some atoms gaining enough energy to exceed the binding energy. Thus the number of ablated atoms below threshold for a single pulse is several times lower than the number of atoms in a monolayer. Thus, the density increase after the single pulse comprises $n_1 \sim 3N_{\text{abl}}/4\pi(R_{\max})^3 \cong 1.5 \times 10^{13} \text{ cm}^{-3}$ in the conditions of our experiments. Hence, more than 10^3 pulses are needed to create a vapor dense enough to “switch on” thermal evaporation in the manner invoked in the presence of air. In fact in our experiments around a thousand pulses on average dwell at the same spot on the target and this may be sufficient to cause some change of the ablation threshold because of an increased level of thermal ablation. The difference between the single pulse and the multiple pulse thresholds is, however, in a range of experimental error in the case of Al, Cu, and Fe. However, the difference for lead is large and it might be explained by the accumulation effect, although as pointed out earlier the physical parameters for lead are not well known especially at elevated temperatures. Evidently, more experimental and theoretical studies needed to understand the difference between the single-pulse and the high-repetition rate multiple-pulse ablation threshold.

IV. CONCLUSIONS

Experiments on the ablation of metals in air and in vacuum by 4.1 MHz repetition rate laser revealed that the presence of air results in a significant reduction in the ablation threshold. In order to explain this observation we have analyzed in detail the role of nonthermal ablation and thermal evaporation for the intermediate duration pulses (12 ps) used in the experiments.

Our analysis shows that for materials such as aluminum, the single pulse threshold in vacuum agrees with the threshold for nonthermal ablation that is the well-accepted mechanism applying to ultrashort pulses. This implies that in vacuum there is a negligible contribution from thermal evaporation both during and after the pulse. The threshold condition then corresponds to the surface atoms receiving energy directly from the laser equal to their binding energy.

The somewhat unexpected conclusion that thermal evaporation is negligible led us to examine in detail the characteristic timescales for energy transfer within the laser-heated layer. In previous models only the electron-to-lattice energy transfer time and the thermal conduction time have been regarded as important. For the materials that were studied we find that, generally, the electron and lattice energies equilibrate close to the end of the 12 ps laser pulse and the heat

conduction time is usually several times longer than the pulse duration, in agreement with previous work. However, when the laser fluence is below the threshold for nonthermal ablation, thermal evaporation will occur only if a Maxwellian distribution of atom energies can be established at the target surface. We show that the time needed to create the Maxwellian distribution at the surface is surprisingly long and is determined by the bulk-to-surface energy transfer time due to collisions between the surface atoms and those in the bulk. In fact the time to equilibrate the surface is at least an order of magnitude longer than in the bulk material and is strongly dependent on the layer temperature.

Thus, for example, when the laser imparts energy to the surface atoms corresponding to half their binding energy, the thermalization time at the surface approaches 100 ps compared with only 1 ps in the bulk. Since the surface thermalization time is now longer than the cooling time of the surface, it becomes impossible for thermal evaporation to contribute to material removal at fluences below the threshold for nonthermal ablation. It is worth noting that we predict thermalization of the surface layer still occurs in a time < 1 ns and hence our results are completely consistent with the many experimental studies of ablation using nanosecond pulses where it is well established that the thermal mechanism dominates.

The clue to understanding why the ablation threshold is lower in air than in vacuum then stems from the need to create a Maxwellian distribution of energies at the surface for thermal evaporation to occur. In this case collisions between the air and the laser-heated surface create of a new pathway by which the surface can thermalize—in fact, the air replaces the role of the saturated vapor in the classical model of thermal evaporation. Whilst it takes up to 1 ns for the air to thermalize with the surface once this occurs thermal evaporation will still result in the removal of a mono layer from the surface at fluences between two and three times lower than the threshold in vacuum. Hence one concludes that the presence of a gaseous atmosphere switches on thermal evaporation that was negligible in vacuum.

It follows from this explanation that the presence of any vapor near the target surface could result in a decrease in the ablation threshold via the same mechanism. We consider the case of the vapor produced when a high repetition rate laser such as used in these experiments is used to continuously evaporate the target. The analysis indicates that the vapor accumulated from multiple pulses hitting the same spot on the target has a density close to the value that might reduce the ablation threshold in our experiments. In particular in the case of lead this might provide a reason for the larger discrepancy between the measured and calculated threshold values.

Further experimental studies, including time-resolved measurements of the dielectric properties, i.e., real and imaginary parts of the dielectric function during the pulse and after the pulse will allow one to gain complete understanding of the ablation processes near and above the ablation threshold.

ACKNOWLEDGMENTS

The support of the Australian Research Council is gratefully acknowledged.

TABLE VI. Optical parameters for metals at room temperature at 532 nm.

	Al	Cu	Fe	Pb ^a
n	0.85	2.60	1.05	2.01
k	6.48	2.58	3.33	3.48
$A=1-R=1-\frac{[(n-1)^2+k^2]}{[(n+1)^2+k^2]}$	0.075	0.487	0.432	0.38
l_s (nm)	13.11	32.85	25.43	24.3
Electron-phonon collision time $t_{e-ph}=\nu_{e-ph}^{-1}$, ps	5.42	9.88	8.5	33.57

^aAt 589.3 nm (Ref. 29).

APPENDIX A: OPTICAL CHARACTERISTICS OF METALS

The values of the temperature to the pulse end and ablation threshold strongly depend on the absorption coefficient and skin depth. Most of the optical parameters of metals are known at the room temperature (see Table VI).

We included in the above table electron-phonon energy exchange rate estimated as the following:

$$\nu_{e-ph} \approx \frac{J_i}{\hbar} \cdot \frac{m_e}{M},$$

where J_i is the ionization potential. Metal is converted to a partially ionized plasma at the ablation threshold, the optical properties are changed, and they are unknown. One can estimate the ratio A/l_s as the following. Near the ablation threshold the condition holds: $\nu_{\text{eff}} \sim \omega_{pe} > \omega$. The dielectric function and the refractive index then are as follows:

$$\varepsilon' \approx \frac{\omega^2}{\omega_{pe}^2}, \quad \varepsilon'' \approx \frac{\omega_{pe}}{\omega} \left(1 + \frac{\omega^2}{\omega_{pe}^2}\right)^{-1}, \quad n \approx k = \left(\frac{\varepsilon''}{2}\right)^{1/2}. \quad (\text{A1})$$

The absorption coefficient then immediately follows from the Fresnel formulas

$$A = 1 - R \approx \frac{4n}{(n+1)^2 + n^2}. \quad (\text{A2})$$

The optical parameters for the ‘‘hot’’ metallic plasma at $\lambda = 532$ nm ($\omega = 3.54 \times 10^{15}$ s⁻¹) are presented in Table VII. The electron heat capacity at $T_e \sim \varepsilon_b < \varepsilon_F$ is also unknown. We interpolate its dependence on $x = T_e/\varepsilon_F$ by the function $C_e \approx \frac{3}{2}(2x - x^2)$ that attains the ideal gas value at $T_e = \varepsilon_F^*$. The electron effective masses for the threshold calculations at $T_e = T_i = \varepsilon_b$ by Eq. (21) were taken equal to those from the

 TABLE VII. The optical parameters for ‘‘hot’’ metallic plasma at $\lambda = 532$ nm.

	Al	Cu	Fe	Pb
$n \sim k$	1.67	1.45	1.81	1.46
A	0.673	0.716	0.648	0.714
l_s , nm	50.7	58.4	46.8	58.0

TABLE VIII. Binding energy and heat capacity.

	Al	Cu	Fe	Pb
Binding energy, eV	3.065	3.173	3.695	1.795
C_e (in units k_B)	0.473	0.76	0.122	0.269

thermal conductivity measurements (see Table VIII).^{14,30}

APPENDIX B

The physical properties of metals used in the experiments are supplied in Table IX.

APPENDIX C: ANALYTICAL FORMULA FOR THE ABLATION DEPTH

Introducing new variable $x = (t/t_{b-s})^{1/4}$, Eq. (24) reduces to the following:

$$l_{\text{th}} = 2t_{b-s} \left(\frac{2T_{bs}}{M}\right)^{1/2} \int_1^\infty \exp\left\{-\frac{\varepsilon_b}{T_{bs}}x^2\right\} x dx^2. \quad (\text{C1})$$

The last integral is integrated by parts:

$$\begin{aligned} & \int_1^\infty \exp\left\{-\frac{4\varepsilon_b}{T_{bs}}x^2\right\} 2x dx^2 \\ & \equiv \int_1^\infty \exp\{-cx^2\} 2x dx^2 \\ & = -\frac{2}{c} \int_1^\infty x d \exp\{-cx^2\} \\ & = -\frac{2}{c} \left\{ x \exp\{-cx^2\} \Big|_1^\infty - \int_{-\sqrt{c}}^\infty \exp\{-u^2\} du \right\} \\ & \approx \frac{T_{bs}}{2\varepsilon_b} \exp\left\{-\frac{4\varepsilon_b}{T_{bs}}\right\}. \end{aligned} \quad (\text{C2})$$

In our case always $c = 4\varepsilon_b/T > 2$. Therefore $\int_{-\sqrt{c}}^\infty \exp\{-u^2\} du \sim 0$. Finally one obtains

$$l_{\text{th}} \approx t_{b-s} \left(\frac{2T_{bs}}{M}\right)^{1/2} \frac{T_{bs}}{2\varepsilon_b} \exp\left\{-\frac{4\varepsilon_b}{T_{bs}}\right\}. \quad (\text{C3})$$

TABLE IX. Physical properties of metals.

	Al	Cu	Fe	Pb
Thickness of mono-layer, 10 ⁻⁸ cm	2.86	2.56	2.35	3.5
Electron density, 10 ²² cm ⁻³	18.6	8.45	16.8	13.2
Atomic density, 10 ²² cm ⁻³	6.02	8.45	8.5	3.3
Fermi energy, eV	11.63	7.0	11.1	9.47
Ionization potential, eV	5.86	7.73	7.9	7.417
Binding energy, eV	3.065	3.173	3.695	1.795
Thermal diffusivity, cm ² /s	0.979	1.165	0.228	0.241
Thermal electron effective mass, m^*/m_e (Refs. 14 and 30)	1.48	1.38	8.0	1.97

*Email address: gam110@rsphysse.anu.edu.au

- ¹P. B. Corkum, F. Brunel, N. K. Sherman, and T. Srinivasan-Rao, *Phys. Rev. Lett.* **61**, 2886 (1988).
- ²B. C. Stuart, M. D. Feit, S. Herman, A. M. Rubenchik, B. W. Shore, and M. D. Perry, *J. Opt. Soc. Am. B* **13**, 459 (1996).
- ³S. Nolte, C. Momma, H. Jacobs, A. Tünnermann, B. N. Chichkov, B. Wellegehausen, and H. Welling, *J. Opt. Soc. Am. B* **14**, 2716 (1997).
- ⁴D. Du, X. Liu, G. Korn, J. Squier, and G. Mourou, *Appl. Phys. Lett.* **64**, 3071 (1994).
- ⁵B. C. Stuart, M. D. Feit, A. M. Rubenchik, B. W. Shore, and M. D. Perry, *Phys. Rev. Lett.* **74**, 2248 (1995).
- ⁶M. D. Perry, B. C. Stuart, P. S. Banks, M. D. Feit, V. Yanovsky, and A. M. Rubenchik, *J. Appl. Phys.* **85**, 6803 (1999).
- ⁷A. M. Malvezzi, N. Bloembergen, and C. Y. Huang, *Phys. Rev. Lett.* **57**, 146 (1986).
- ⁸B. Luther-Davies, E. G. Gamaly, Y. Wang, A. V. Rode, and V. T. Tikhonchuk, *Sov. J. Quantum Electron.* **22**, 289 (1992).
- ⁹K. Eidmann, J. Meyer-ter-Vehn, T. Schlegel, and S. Huller, *Phys. Rev. E* **62**, 1202 (2000).
- ¹⁰E. G. Gamaly, A. V. Rode, B. Luther-Davies, and V. T. Tikhonchuk, *Phys. Plasmas* **9**, 949 (2002).
- ¹¹V. Z. Kolev, M. J. Lederer, B. Luther-Davies, and A. V. Rode, *Opt. Lett.*, **28**, 1275 (2003).
- ¹²B. Luther-Davies, V. Z. Kolev, M. J. Lederer, N. R. Madsen, A. V. Rode, J. Gieseke, K.-M. Du, and M. Duering, *Appl. Phys. A: Mater. Sci. Process.* **79**, 1051 (2004).
- ¹³M. I. Kaganov, I. M. Lifshitz, and L. V. Tanatarov, *Sov. Phys. JETP* **4**, 173 (1957).
- ¹⁴C. Kittel, *Introduction to Solid State Physics* (Wiley & Sons, New York, 1996).
- ¹⁵Ya. B. Zel'dovich and Yu. P. Raizer, *Physics of Shock Waves and High-Temperature Hydrodynamic Phenomena* (Dover, New York, 2002).
- ¹⁶L. D. Landau and E. M. Lifshitz, *Statistical Physics* (Pergamon, Oxford, 1980).
- ¹⁷W. L. Kruer, *The Physics of Laser Plasma Interaction* (Addison Wesley, New York, 1987).
- ¹⁸W. M. MacDonald, M. N. Rosenbluth, and W. Chuck, *Phys. Rev.* **107**, 350 (1957).
- ¹⁹A. Zangwill, *Physics at Surfaces* (Cambridge University Press, Cambridge, 1988).
- ²⁰M. Prutton, *Introduction to Surface Physics* (Clarendon, Oxford, 1994).
- ²¹Yu. V. Afanasiev and O. N. Krokhin, in *Physics of High Energy Density*, Proceedings of the International School of Physics "Enrico Fermi," Course XLVIII, edited by P. Calderola and H. Knoepfel (Academic, New York, 1971).
- ²²S. I. Anisimov, Ya. A. Imas, G. S. Romanov, and Yu. V. Khodyko, *Action of High Intensity Radiation on Metals* (National Technical Information Service, Springfield, VA, 1971).
- ²³*Handbook of Optics*, edited by M. Bass, E. W. Van Stryland, D. R. Williams, and W. L. Wolfe (McGraw-Hill, New York, 2001), Vol. 2.
- ²⁴D. von der Linde, H. Schuler, *J. Opt. Soc. Am. B* **13**, 216 (1996).
- ²⁵O. P. Uteza, E. G. Gamaly, A. V. Rode, M. Samoc, and B. Luther-Davies, *Phys. Rev. B* **70**, 054108 (2004).
- ²⁶T. Itina (private communication).
- ²⁷Yu. P. Raizer, *Laser-Induced Discharge Phenomena* (Consultants Bureau, New York, 1977), p. 91.
- ²⁸*CRC Handbook of Chemistry and Physics*, 60th ed., edited by R. C. Weast and M. J. Astle (CRC, Boca Raton, 1980).
- ²⁹M. Born and E. Wolf, *Principles of Optics: Electromagnetic Theory of Propagation, Interference, and Diffraction of Light*, 7th ed. (Cambridge University Press, Cambridge, 2002), p. 746.
- ³⁰N. W. Ashcroft and N. D. Mermin, *Solid State Physics* (Holt-Saunders, New York, 1976), p. 48.